Investigation of Cooling Performances of a Non-Film-Cooled Turbine Vane Coated with a Thermal Barrier Coating Using Conjugate Heat Transfer

Prasert Prapamonthon [1,2,*], Soemsak Yooyen [1], Suwin Sleesongsom [1], Daniele Dipasquale [1], Huazhao Xu [3], Jianhua Wang [3] and Zhaoqing Ke [4]

[1] Department of Aeronautical Engineering, International Academy of Aviation Industry, King Mongkut's Institute of Technology Ladkrabang, Bangkok 10520, Thailand; soemsak.yo@kmitl.ac.th (S.Y.); suwin.se@kmitl.ac.th (S.S.); daniele.di@kmtil.ac.th (D.D.)

[2] Key Laboratory for Mechanics in Fluid Solid Coupling Systems, Institute of Mechanics, Chinese Academy of Sciences, Beijing 100190, China

[3] Department of Thermal Science & Energy Engineering, School of Engineering Science, University of Science and Technology of China, Hefei 230027, China; xuhz@ustc.edu.cn (H.X.); jhwang@ustc.edu.cn (J.W.)

[4] Department of Mechanical and Aerospace Engineering, College of Engineering, University of Missouri-Columbia, Columbia, MO 65211, USA; kezh@missouri.edu

* Correspondence: prasert.pr@kmitl.ac.th or jinfa@imech.ac.cn; Tel.: +66-81-4899-546

Abstract: The aim of this paper is to numerically investigate cooling performances of a non-film-cooled turbine vane coated with a thermal barrier coating (TBC) at two turbulence intensities (Tu = 8.3% and 16.6%). Computational fluid dynamics (CFD) with conjugate heat transfer (CHT) analysis is used to predict the surface heat transfer coefficient, overall and TBC effectiveness, as well as internal and average temperatures under a condition of a NASA report provided by Hylton et al. [NASA CR-168015]. The following interesting phenomena are observed: (1) At each Tu, the TBC slightly dampens the heat transfer coefficient in general, and results in the quantitative increment of overall cooling effectiveness about 16–20%, but about 8% at the trailing edge (TE). (2) The protective ability of the TBC increases with Tu in many regions, that is, the leading edge (LE) and its neighborhoods on the suction side (SS), as well as the region from the LE to the front of the TE on the pressure side (PS), because the TBC causes the lower enhancement of the heat transfer coefficient in general at the higher Tu. (3) Considering the internal and average temperatures of the vane coated with two different TBCs, although the vane with the lower thermal conductivity protects more effectively, its role in the TE region reduces more significantly. (4) For both TBCs, the increment of Tu has a relatively small effect on the reduction of the average temperature of the vane.

Keywords: turbine vane; heat transfer coefficient; thermal barrier coating; turbulence intensity; conjugate heat transfer

1. Introduction

The performance of a gas turbine engine is evaluated by two thermomechanical quantities, that is, thermal efficiency and output power. A key factor to obtain this performance is that turbines' airfoils need to be able to operate under serious circumstances from high thermal loads at the turbine inlet. Therefore, thermal barrier coatings (TBCs) and cooling techniques (internal cooling and film cooling) are widely used in advanced gas turbines to thermally protect the airfoils, to maintain and prolong a useful life of the airfoils, from the turbine inlet temperature (TIT). However, the cooling techniques are

limited by cooling air consumption. Hence, TBC is essential for the airfoils as an insulator to avoid direct contact with hot gases. In fact, several factors may influence the protective ability of TBC, that is, thermal conductivity, thickness, porosity, phase stability, surface roughness of the TBC, temperature of the hot gas, matching of thermal expansion coefficients with the metal surface coated with TBC, and coating method. Meier and Gupta [1] highlighted that the TBC could be applied to reduce the surface temperature of a turbine part by 167 °C. Maikell et al. [2] experimentally investigated the TBC effect on overall effectiveness of a leading-edge model based on cylindrical geometry. They found that at the interface of the TBC, the TBC significantly increased overall effectiveness. Boyle [3] studied the effects of TBC on improving the thermal efficiency of an engine; he concluded that TBC had an impact on vane sensitivity to the external heat transfer coefficient. Boyle and Senyitko [4] indicated that the presence of TBC added the skin roughness, which was a physical factor of TBC, and had significant results on the heat transfer rate on the turbine vane surface.

Recently, the technique of computational fluid dynamics (CFD) with fluid–solid interaction analysis, also called conjugate heat transfer (CHT), has been commonly used by many researchers [5–9] to obtain a better understanding of the phenomena of fluid flow and heat transfer happening from fluid–solid interfaces in gas turbine engines. Furthermore, CHT analysis has been applied to predict the effect of TBC on thermal and mechanical phenomena of turbine airfoils, also, Na et al. [10] used CHT analysis with realizable k–ε turbulence to study the effects of TBC on a flat plate model with cylindrical holes. They indicated that TBC reduced the lateral conductive heat transfer of the surface. Also, TBC made temperature gradients more discrete under the coolant jets. Bohn and Becker [11] both aerodynamically and thermally investigated the Mark II vane reported by Hylton et al. [12], the vane without TBC and with TBC with a constant thickness of 0.3 mm of ZrO_2, using a 3D CHT approach with the Baldwin–Lomax turbulence model [13]. They found that TBC resulted in the reduction of the surface temperaturesabout 27–43 K in the shock area on the suction side (SS) and about 20–29 K in the stagnation area. With the same simulation technique, Bohn and Tümmers [14] expanded their work by studying thermal stresses in the vane under the effects of mass flow rate of coolant and TBC. They used the Mark II vane coated with two layers of TBC: a constant thickness of 0.125 mm of ZrO_2 as the top coat (TC) and 0.06 mm of MCrAlY as the bond coat (BC). They indicated that the influence of the TBC was significantly higher than that of the reduction of coolant mass flow. Alizadeh et al. [15] investigated the effects of thermal conductivity and thickness of TBC on the temperature sensitivity of a turbine blade with internal cooling, using CHT analysis with the SST k–ω model. They concluded that the inclusion of a 0.2-mm thickness of TBC resulted in a 34 K and 19 K drop in the maximum and average blade temperatures, respectively. Moreover, the blade average temperature could be increased about 10 K when the thermal conductivity of the TBC changed from 1 W/m·K to 3 W/m·K. Yongbin et al. [16] used CHT analysis with an SST k–ω model to investigate the effects of TBC and the mass flow rate of cooling air on a gas turbine blade coated with a uniform TBC thickness of 0.3 mm. Their results indicated that the TBC effect was weakened in the trailing edge (TE), but the TBC played a major role in the region cooled effectively by internal cooling. Rossette et al. [17] used CHT analysis with the turbulence model of Spalart–Allmaras [18] to aerodynamically and thermally investigate the performances of a gas turbine blade coated with TBC. They concluded that the inclusion of a thickness of about 100–400 μm of TBC reduced the surface temperature of the blade by as much as 200 °C, and using TBC reduced 36% of the coolant need to maintain the creep life of the blade material.

Incidentally, one recognizes that turbulence intensity (*Tu*) and turbulence length scale (*Lu*) are physical factors that play prominent roles in the performance of a film-cooled turbine airfoil and flow field. In fact, real gas turbine engines are frequently run under *Tu* by about 10% to 20%, as predicted by Mayhew et al. [19]. Effects of *Tu* on the performance of film cooling of the turbine vanes and blades, flat plate, and cylindrical leading-edge models were numerically and experimentally investigated by many groups of researchers [20–28]. However, few experimental and numerical studies have hitherto been focused on a real situation regarding the cooling performances of turbine airfoils from simultaneous effects of TBC and *Tu*. Davidson et al. [29] experimentally investigated TBC and film cooling on the C3X

scaled up 12× at *Tu* = 0.5% and 20%. Their results indicated that with no film cooling, TBC increased the overall effectiveness by as much as 200%. When *Tu* increased from 0.5% to 20%, overall effectiveness changed insignificantly. For the film-cooled vane with round holes, overall effectiveness was increased significantly by TBC, and the effect of the blowing ratio on the overall cooling effectiveness of the turbine vane with TBC was minimal. Prapamonthon et al. [30,31] simultaneously studied the effects of *Tu* and TBC on the cooling performance of a leading-edge cooling guide vane and a real film-cooled vane, using 3D CHT analysis at *Tu* = 3.3%, 10%, and 20%. Their works indicated that TBC was more effective when the level of *Tu* increased. Namely, at *Tu* = 20% with film cooling, overall effectiveness was improved as much as about 24% in the regions cooled ineffectively. For the leading-edge cooling guide vane, overall cooling effectiveness at the hub increased by about 25%.

Hence, there is a demand to provide gas turbine engineers and designers with useful numerical studies of real phenomena from the effects of *Tu* and TBC on the cooling performance of a turbine airfoil. This research proposes a numerical investigation of the cooling performance of the C3X vane, an extensively non-film-cooled turbine vane reported by Hylton et al. [12], coated with TBC at different *Tu*s using the analysis of 3D CHT linked with CFD.

2. Thermal Parameters

The evaluation method of four thermal parameters which relate to temperatures on the metal surface with and without TBC is demonstrated in Figure 1, as established by Prapamonthon et al. [31]. The presence of a bond coat is neglected by a simplified assumption that it is a part of the vane surface with a relatively thin thickness. Thus, its thermal resistance on heat transfer through the vane surface is disregarded.
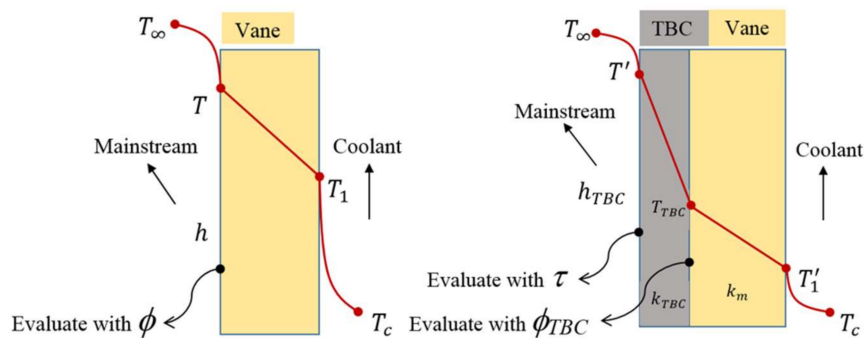
Figure 1. Evaluation of the thermal parameters used in this work [31]. TBC: thermal barrier coating.

(1) Heat transfer coefficient (*h*):

$$h = \frac{q_{flux}}{T_\infty - T_w} \tag{1}$$

where $T_w = \begin{cases} T, \text{without TBC} \Rightarrow h \\ T', \text{with TBC} \Rightarrow h_{\text{TBC}} \end{cases}$, if *h* is positive, it means that heat flux transfers into the solid structure. On the other hand, if heat flux transfers into the fluid, *h* is negative. However, in this work, *h* is expected to be positive because $T_\infty > T_w$.

(2) Overall cooling effectiveness (*φ*):

$$\varphi = \frac{T_\infty - T_w}{T_\infty - T_c} \tag{2}$$

where $T_w = \begin{cases} T, \text{without TBC} \Rightarrow \varphi \\ T_{\text{TBC}}, \text{with TBC} \Rightarrow \varphi_{\text{TBC}} \end{cases}$, with a conduction wall and CHT analysis, the cooling performance on the vane metal surface is evaluated by this parameter.

(3) Thermal barrier coating effectiveness (τ):

$$\tau = \frac{T_\infty - T'}{T_\infty - T_c} \tag{3}$$

The effect of TBC on the cooling performance is discussed by this parameter through the external surface of TBC.

(4) Percentage of metal temperature reduction (R):

$$R = \left(1 - \frac{T_{\text{TBC}}}{T}\right) \times 100\% \tag{4}$$

This parameter is used to consider the TBC ability to protect the metal surface from the hot gas.

3. Geometric Configuration

In this work, the geometry of the C3X vane reported by Hylton et al. [12] is used. Figure 2 depicts the mainstream cascade, the configuration of the C3X vane with a constant cross section, and ten cylindrical cooling passages where air flows from the hub to the tip. Its height is 76.2 mm in the spanwise direction.
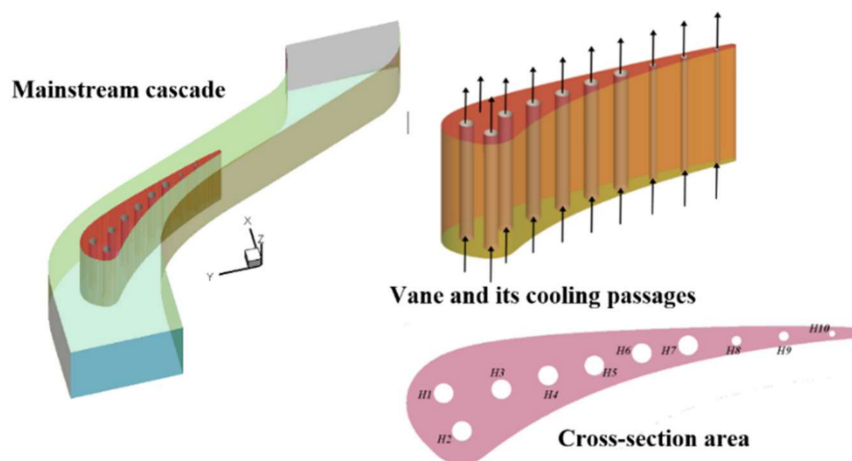

Figure 2. Mainstream cascade and C3X geometric configuration and its cross-section area at midspan.
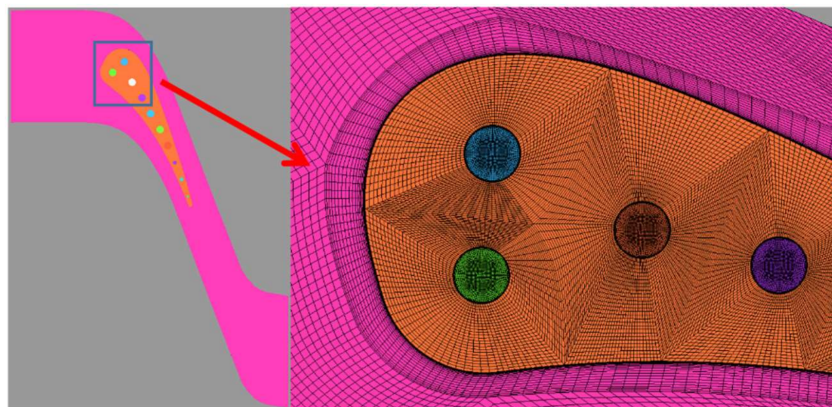
4. Computational Setup

4.1. Computational Mesh and Mesh Independence

In this work, computational meshes are generated by ICEM, ANSYS V.15. In order to obtain simple and high-quality meshes, all computational domains are formed as hexahedral unstructured meshes. All meshes are improved by the O-grid technique to attain high-quality meshes and suffice to resolve the boundary layer near surfaces in fluid domains. The value of y+ for the computational mesh of the first cell is less than 5. Comparisons of the distributions of surface temperatures along the vane surface at midspan with three mesh number strategies, that is, 4,834,244 (4.8 M, coarse mesh), 5,574,920 (5.5 M, medium mesh), and 6,655,148 (6.6 M, fine mesh), are considered to confirm mesh independence. Figure 3 shows that most of the numerical results of 5.5 M and 6.6 M give a very good agreement, with the maximum error about 1%. Therefore, it is not necessary to increase the quantity of mesh elements, and the 5.5 M is selected as the computational mesh throughout the following calculations.
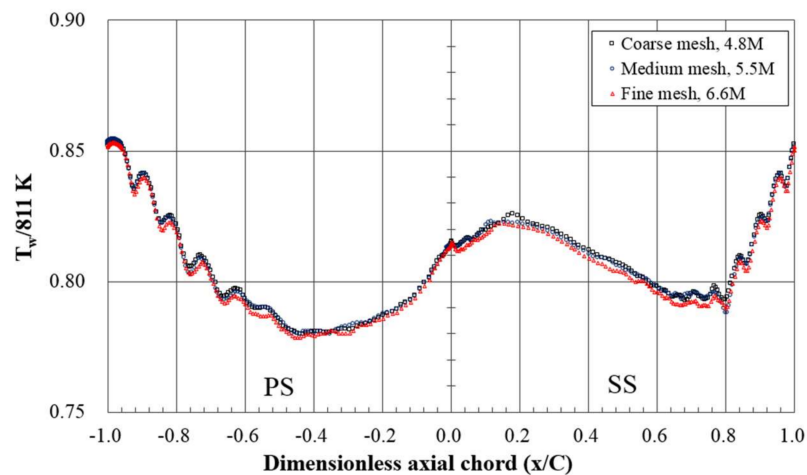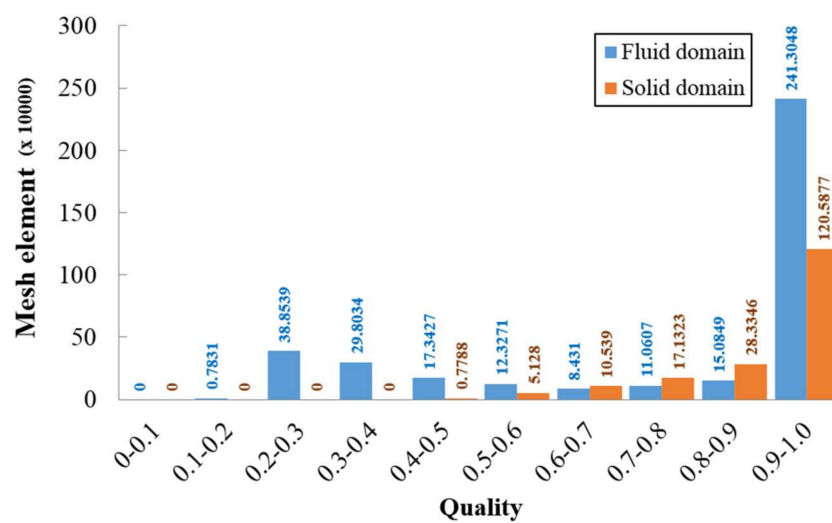
Figure 3. Comparisons of three mesh number strategies for surface temperature distributions at midspan. PS: pressure side; SS: suction side.

Figures 4 and 5 show a part of the generated mesh of the solid and fluid domains, and the mesh quality distributions of the solid and fluid domains, respectively.


Figure 4. Computational mesh shown at midspan.

Figure 5. Mesh quality distributions.

4.2. Techniques of Calculation

Numerical results in this research are conducted by using ANSYS FLUENT v15 under the appropriate implementation of the pressure-based segregated algorithm with the SIMPLE method and SST k–ω turbulence model. The second-order accuracy of the discretization scheme is determined in the solid and fluid regions. The convergence process and its stability are improved by under-relaxation factors, and the accuracy of the results is furthered by an option of low-Reynolds number corrections for low speed flows and four correction factors for the compressibility effect, curvature correction, viscous heating, and production limiter. The convergence criteria are that the residuals of the scaled continuity and energy equations must be lower than 10^{-3} and 10^{-6}, respectively. To confirm the convergence of the numerical results, the mass-flow-rate balance at all inlets and outlets is checked carefully. Moreover, the six-point temperatures on the vane surface are monitored until the larger changes of these parameters disappear with subsequent iterations. As per previous works done by Prapamonthon [30,31], it is expected that the converged solutions are obtained after 17,000–18,000 iterations. With CHT analysis, the Navier–Stokes equations and equation of energy are solved within the fluid domain, whereas the heat conductive equation by Fourier's law is only solved in the solid domain under a suitable thermal conductive effect to associate the calculation of heat flux. The mesh interface technique (MIT) with the couple wall option is exploited at all interfaces of the solid and fluid domains to allow heat flux to transfer at the interfaces, whereas fluid cannot flow across these interfaces, as presented in Figure 6a.
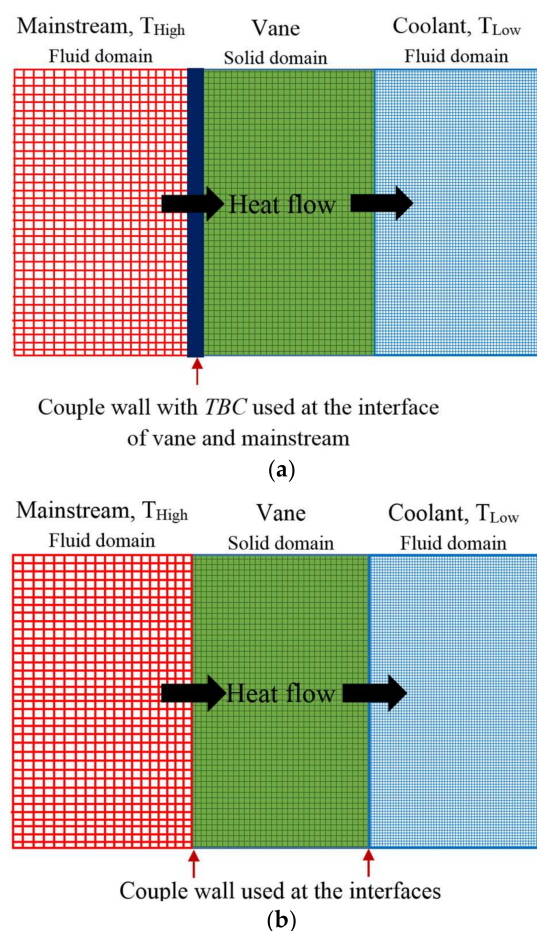
Figure 6. Interface technique with a couple wall, (**a**) without and (**b**) with thermal barrier coating (TBC) [30,31].

To consider the effect of TBC at all interfaces, a constant thickness of 0.03556 cm of yttria-partially-stabilized zirconia (ZrO_2) is used as a TBC insulator, as used by Halila et al. [32], and named as TBC 1. Figure 6b illustrates the application of the thermal condition provided by FLUENT to address the TBC effect at the interfaces of the solid and fluid domains. Due to a very thin layer of TBC, only 1D heat conduction is considered in the TBC. In order to further study the thermally protective effect of TBC, a new TBC proposed by Wang et al. [33] is used as the candidate TBC, named as TBC 2. Table 1 gives the important properties of the TBC materials used to take account of the heat conduction through TBC.

Table 1. Properties of TBC materials.

Property	TBC 1: ZrO_2 (YSZ)	TBC 2: $La_{1.7}Dy_{0.3}Zr_2O_7$ (LDZ) (based on Wang et al. [33,34])
Density	ρ_{TBC} = 5500 kg/m^3	ρ_{TBC} = 5600 kg/m^3
Specific heat capacity	c_{TBC} = 418 J/kg·K	c_{TBC} = 0.9472T + 135.6 J/kg·K
Thermal conductivity	k_{TBC} = 1.04 W/m·K, in the range suggested by Feuerstein et al. [35]	k_{TBC} = 0.468 W/m·K

Air is used as the mainstream and the coolant in the passages, and the vane structure is assumed as being made of steel, and their properties in this work are given in Table 2.

Table 2. Material properties.

Material Property	Fluid domains: Air (Coolant and Mainstream)	Solid domain: Steel (Vane)
Density	ρ_f = Ideal gas assumption	ρ_m = 7854 kg/m^3
Specific heat capacity	c_f = 1004.4 J/kg·K	c_m = 434 J/kg·K
Thermal conductivity	k_f = 0.0261 W/m·K	Linear correlation: k_m (W/m·K) = 6.811 + 0.020176T
Viscosity	ν_f = 1.7831 × 10^{-5} kg/m·s	-

4.3. Boundary Conditions

In this work, the boundary conditions of the external mainstream and internal coolant passages are set as those of the run number 4112 of the experiment reported by Hylton et al. [12] at *Tu* = 8.3% and 16.6% as given in Tables 3 and 4, respectively. However, it should be noted that this research is conducted under a simple assumption that any physical change in the faces of TBC, which may occur in any experiment, is not considered.

Table 3. Boundary conditions of the external mainstream.

| Boundary	Condition
Mainstream inlet	T_∞ = 783 K, $P_{t,in}$ = 321.7 kPa, *Tu* = 8.3% and 16.6%
Mainstream outlet	$P_{s,out}$ = 192.5 kPa
All coolant inlets	Mass flow inlet with different mass flow rates as shown in Table 4
All coolant outlets	P = 100 kPa
Upper and lower cascades	Adiabatic wall with nonslip condition
Lateral cascade	Periodic

Table 4. Boundary conditions of the internal coolant passages.

Coolant Passage Number	T_c (K) Based on Refs. [5–7]	Mass Flow Rate (kg/s)
H1	387	0.0078
H2	388	0.0066
H3	371	0.0063
H4	376	0.0067
H5	355	0.0065
H6	412	0.0067
H7	367	0.0063
H8	356	0.0023
H9	406	0.0014
H10	420	0.00068

4.4. Validation of Turbulence Model

The experimental data reported by Hylton et al. [12] is used to validate the numerical results of the pressure and surface temperature at midspan obtained by the SST k–ω turbulence model, as presented in Figure 7. From Figure 7a, it is obvious that the SST k–ω model predicts a good pressure distribution compared to the experimental data. Only a slight difference happens on the SS in the range of 0.7 < x/C < 0.9. Besides, this turbulence model overestimates the surface temperature in the range of −0.7 < x/C < 0.4, and underestimates in the two ranges of −1.0 < x/C < −0.7 and 0.4 < x/C < 1.0, as seen in Figure 7b. However, the model gives the trend of the surface temperature distribution well, with the maximum error about 3%. So, it is acceptable and reasonable to use the SST k–ω model in the following simulations.


(a)　　　　　　　　　　　　　　　　　　　(b)
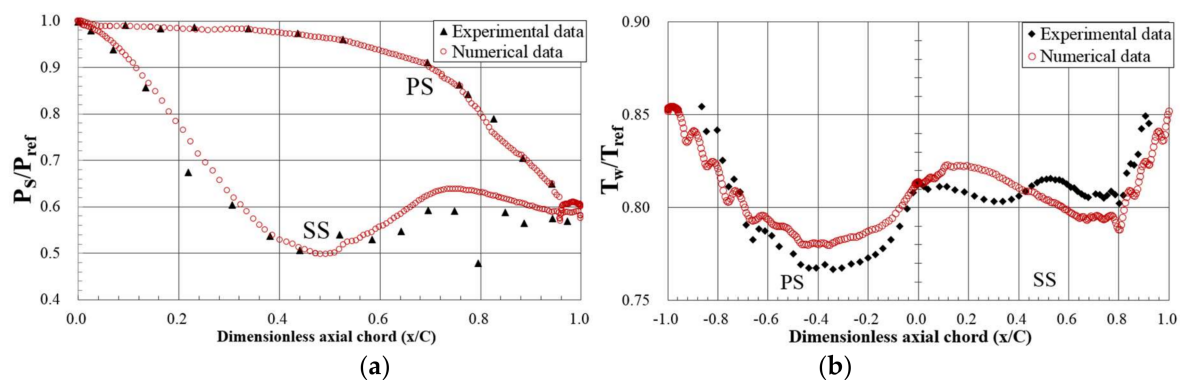
Figure 7. Comparisons between experimental and numerical results at midspan (**a**) pressure and (**b**) temperature distributions.

5. Results and Discussions

5.1. Percentage of Metal Temperature Reduction

Figure 8 presents the distributions of the surface temperature reduction (R) at midspan, which indicates that at both *Tu* values, TBC plays a major role in thermal protection in the range of about −0.65 < x/C < 0.8, and TBC can reduce the metal surface temperature by as much as 3.2% (about 25 K) at x ≈ −0.45 on the PS and *Tu* = 16.6%. However, R drops dramatically near the TE, that is, the range of −1.0 < x/C < −0.65 on the PS and 0.8 < x/C < 1.0 on the SS. With increasing *Tu*, R distribution at *Tu* = 16.6% has a similar trend to that at *Tu* = 8.3%. However, R rises in the range of −0.65 < x/C < 0.2 and stays unchanged in the other regions. These phenomena suggest that although the TBC is effective in protecting the metal surface, the role of the TBC in the TE is small because the T_{TBC} is a little lower than T in such regions. This phenomenon may be explained by the fact that the TE is the smallest and thinnest part of the vane, so it is coated with the smallest amount of TBC. Moreover, this region obtains

relatively high temperatures, but is cooled by the lower rates of coolant with the relatively high inlet temperatures, namely, the holes H9 and H10 seen in Figure 2, and Table 4. Additionally, the protective ability of TBC increases with *Tu* in the LE and its neighborhood on the SS, as well as the region from the LE to the front of the TE on the PS, but hardly changes in the other regions.
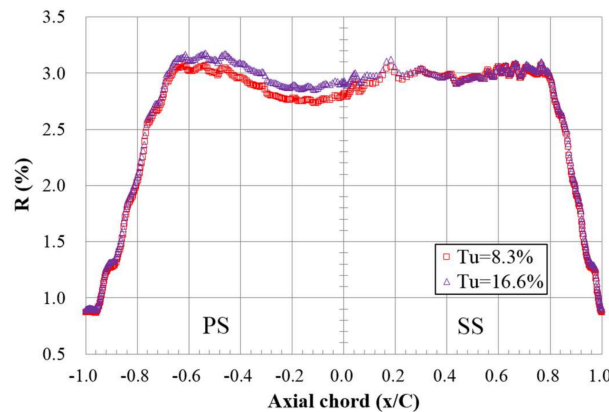

Figure 8. Effects of turbulence intensity (*Tu*) and TBC on surface temperature reduction (*R*) at midspan.
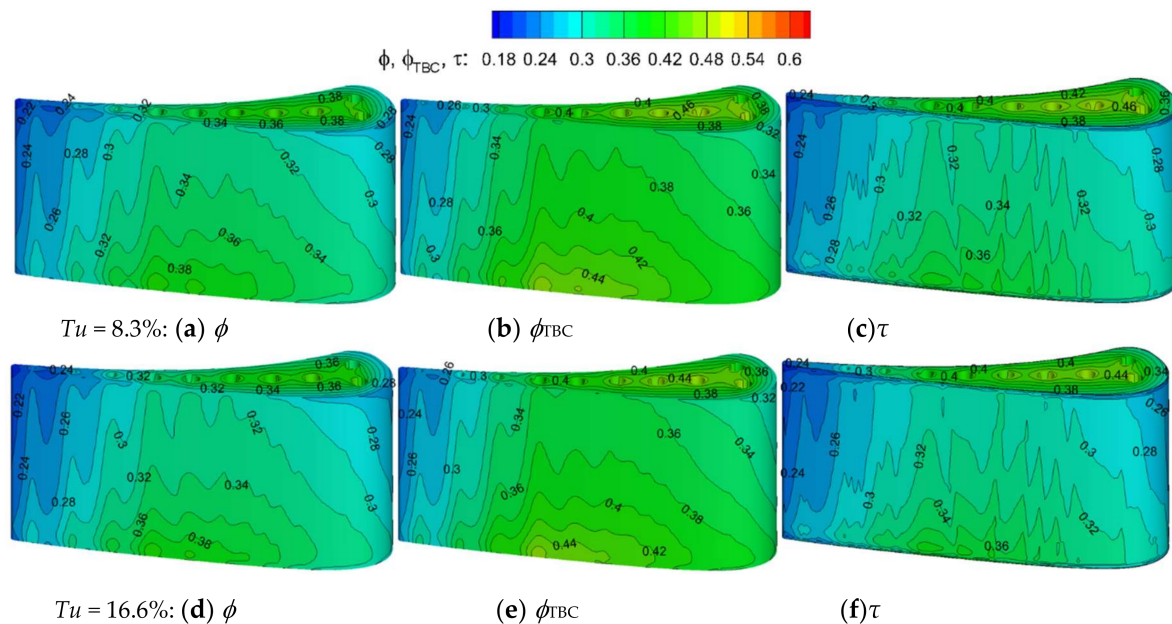
5.2. Overall and TBC Effectiveness

Figure 9 shows comparisons between φ, φ_{TBC}, and τ distributions at midspan for two *Tu*s. At each *Tu*, it is clear that $\tau < \varphi < \varphi_{TBC}$ because $T' > T > T_{TBC}$. The trends of φ, φ_{TBC}, and τ distributions are similar to one another. The maximum φ, φ_{TBC}, and τ are located at the same position, that is, at x/C = −0.45 on the PS. This is reasonable because it is the closest position to the coolant passage H5, where has the lowest inlet temperature and a relatively higher coolant flow rate, as seen in Table 4. With the increase in *Tu*, it is observed that φ, φ_{TBC}, and τ decrease due to the fact that T, T_{TBC}, and T' increase with *Tu*. Another observation is that the reductions of φ, φ_{TBC}, and τ with *Tu* are very small near the TE. The general trends of the characteristics of overall and TBC effectiveness distributions at different *Tu*s are captured by the contours in Figures 10 and 11. The contours indicate that at each *Tu*, the inclusion of TBC leads to the quantitative increment of overall cooling effectiveness by about 16% to 20%, and about 8% at the TE. The reduction of φ_{TBC} is lower than that of φ when *Tu* increases. The reason is that the presence of TBC mitigates the reduction of overall cooling effectiveness by significantly reducing TBC effectiveness on the external surface of the TBC.
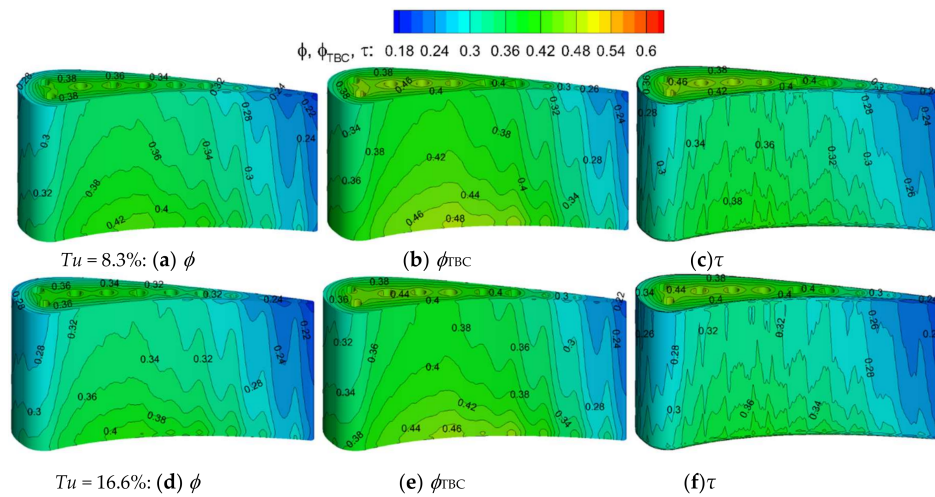

(a)

Figure 9. *Cont.*

(**b**)

(**c**)
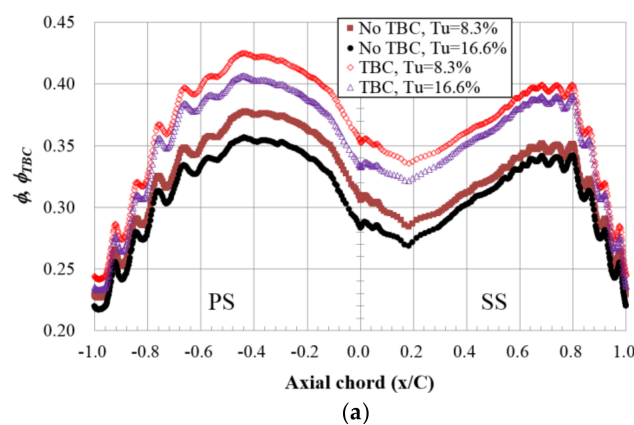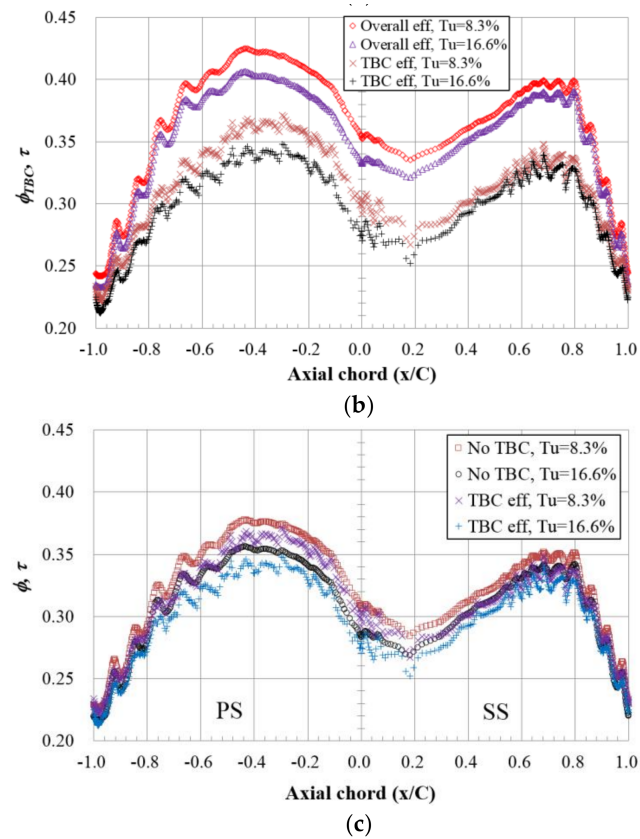
Figure 9. Effects of *Tu* and TBC on φ, φ_{TBC}, and τ distributions at midspan in comparisons between (**a**) φ and φ_{TBC}, (**b**) φ_{TBC} and τ, and (**c**) φ and τ.

Tu = 8.3%: (**a**) ϕ　　　　　　　　(**b**) ϕ_{TBC}　　　　　　　　(**c**)τ

*Tu* = 16.6%: (**d**) ϕ　　　　　　　　(**e**) ϕ_{TBC}　　　　　　　　(**f**)τ

Figure 10. φ, φ_{TBC}, and τ on the suction side (SS) at *Tu* = 8.3% and 16.6%.

Figure 11. φ, φ_{TBC}, and τ on the pressure side (PS) at *Tu* = 8.3% and 16.6%.
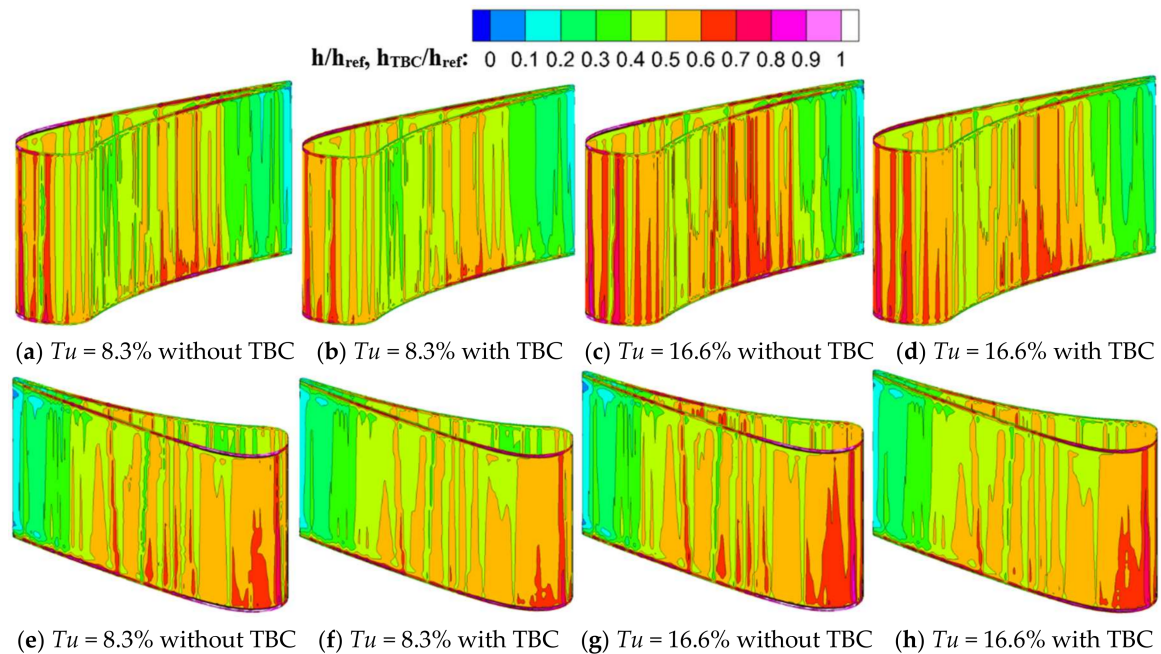
5.3. Heat Transfer Coefficient

Figure 12a,b show the *h* and h_{TBC} distributions at midspan and at the same *Tu* for two *Tu*s, respectively. One can observe that at each *Tu*, *h* and h_{TBC} have similar trends and match the distributions of *R*. Another observation is that h_{TBC} is lower than or equal to *h*, and both *h* and h_{TBC} decrease near the TE. Figure 12c,d present comparisons of *h* and h_{TBC} at midspan and at two *Tu*s, respectively. It is clear that when *Tu* rises up from 8.3% to 16.6%, both *h* and h_{TBC} increase in the range of $-0.75 < x/C < 0.3$, but the increment of *h* is stronger than that of h_{TBC}. However, the effects of increasing *Tu* on *h* and h_{TBC} are slight in the other regions. These phenomena suggest that the heat transfer coefficient may be slightly dampened by TBC and that TBC causes the lower augmentation of the heat transfer coefficient in the LE and its neighborhoods on the SS, as well as the region from the LE to the front of the TE on the PS when the level of *Tu* rises.
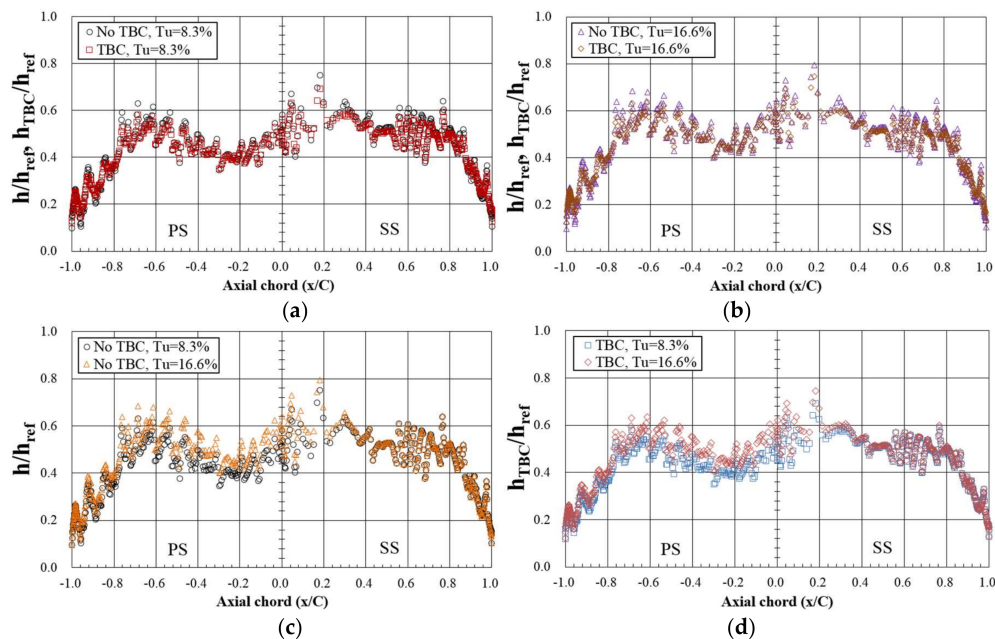
Figure 12. *h* and h_{TBC} distributions at midspan at *Tu* = 8.3% and 16.6% in comparisons between (**a**) *h* and h_{TBC} at *Tu* = 8.3%, (**b**) *h* and h_{TBC} at *Tu* = 16.6%, (**c**) *h* at *Tu* = 8.3% and 16.6%, and (**d**) h_{TBC} at *Tu* = 8.3% and 16.6%.

The overall effects of TBC on h and h_{TBC} at the different *Tu*s are illustrated by holistic contours in Figure 13. It confirms that the inclusion of TBC slightly dampens the heat transfer coefficient and causes the reduction of the heat transfer coefficient in general; that is, $h_{TBC} < h$. However, the trends of h and h_{TBC} distributions are similar to each other. At different *Tu*s, the increase in *Tu* is the cause of increases in h and h_{TBC}, but the augmentation of h_{TBC} remains lower than that of h in general.


(**a**) *Tu* = 8.3% without TBC　(**b**) *Tu* = 8.3% with TBC　(**c**) *Tu* = 16.6% without TBC　(**d**) *Tu* = 16.6% with TBC

(**e**) *Tu* = 8.3% without TBC　(**f**) *Tu* = 8.3% with TBC　(**g**) *Tu* = 16.6% without TBC　(**h**) *Tu* = 16.6% with TBC

Figure 13. Contours of h and h_{TBC} at *Tu* = 8.3% and 16.6%.
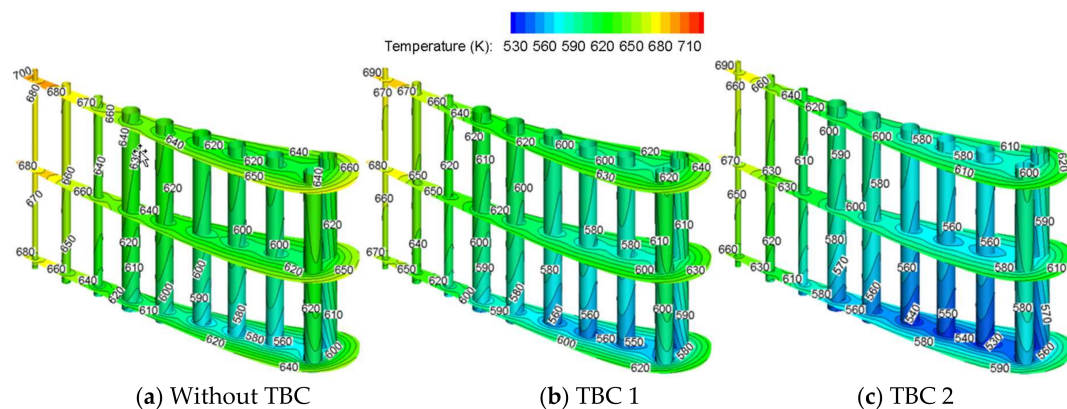
5.4. Vane Internal Temperature

In order to further study of the effect of TBC on cooling performance, the different TBCs, that is, TBC 1 and TBC 2, are used to evaluate the temperature within the vane material in this section. At first, distributions of *R* on the vane surface with TBC 1 and TBC 2 are considered, as depicted in Figure 14. One can observe that TBC 2 gives a higher *R* than TBC 1, and the highest *R* of TBC 2 is about 6.5% if *Tu* = 16.6%, but about 3.2% for TBC 1 at the same *Tu*. However, *R* obtained by TBC 2 drops more severely than that by TBC 1 in the range of $-1.0 < x/C < -0.65$ on the PS and $0.8 < x/C < 1.0$ on the SS, namely, 6.5% to 2% for TBC 2 and 3% to 1% for TBC 1. Also, there is no significant difference of R in such regions, though *Tu* increases. This indicates that although the lower thermal conductivity of TBC protects the vane surface more effectively, at the same time, the role of TBC in the TE region and its vicinity decreases more seriously. Moreover, it is likely that *R* obtained by both TBCs is independent of *Tu* in such regions as well.
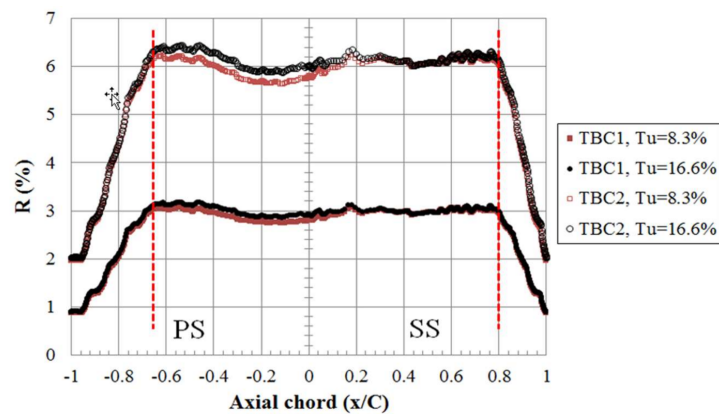
Figure 14. Percentage of metal temperature reduction (*R*) of two TBCs at midspan and *Tu* = 8.3% and 16.6%.

Next, the vane internal temperatures with the two different TBCs are compared against those without TBC using the contours of three-section planes at three spans, that is, 10%, 50%, and 90%, as illustrated in Figures 15 and 16 for *Tu* = 8.3% and 16.6%, respectively. From these figures, it is indicated that the vane internal temperature increases with the spanwise direction, following the direction of coolant flowing in the 10 passages. Another phenomenon is that the relatively high temperatures inside the vane are still observed in the TE region of each section area, although TBC with a lower thermal conductivity is employed. This corresponds to the lowest cooling effectiveness happening on the surface of the TE, including the role of TBC in this region. With the increment of *Tu*, overall and TBC effectiveness decreases as described previously. Hence, the vane surface and internal temperatures increase.

(**a**) Without TBC　　　(**b**) TBC 1　　　(**c**) TBC 2

Figure 15. Contours of vane internal temperature of at *Tu* = 8.3%.

(**a**) Without TBC　　　(**b**) TBC 1　　　(**c**) TBC 2
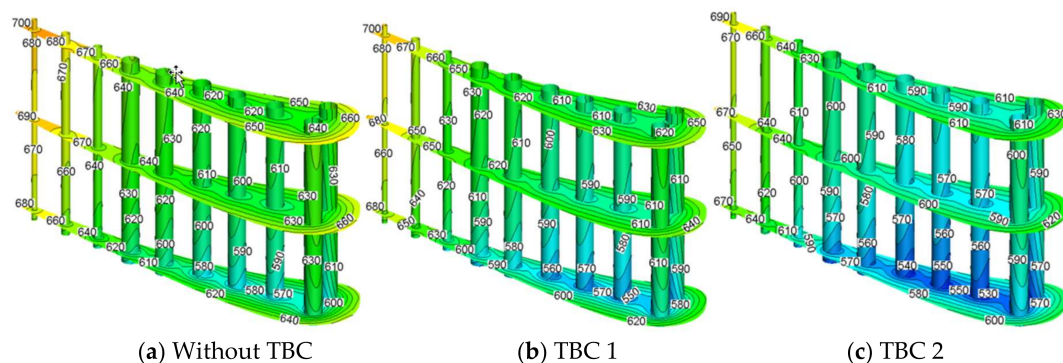
Figure 16. Contours of vane internal temperature of at *Tu* = 16.6%.

Figure 17 shows the effect of TBC on reductions of the average vane temperature at *Tu* = 8.3% and 16.6%. It should be noted that the "average vane temperature" is the volume-average temperature of the vane. The negative value on the ordinate means that TBC reduces the average vane temperature. It is found that TBC 2 reduces the average vane temperature about two times more than TBC 1 (about 38% for TBC 2 and 19% for TBC1), due to its lower thermal conductivity. However, the effect of *Tu* on this reduction is very slight for both TBCs. This may be explained by the fact that the heat transfer coefficient increases with *Tu* as shown in Figure 12c,d, so the average vane temperature increases. Nevertheless, it is found that the increment of the average vane temperature obtained without TBC, TBC 1, and TBC 2 are similar to each other. So, the reductions of the average vane temperature for both TBCs change insignificantly when *Tu* increases.
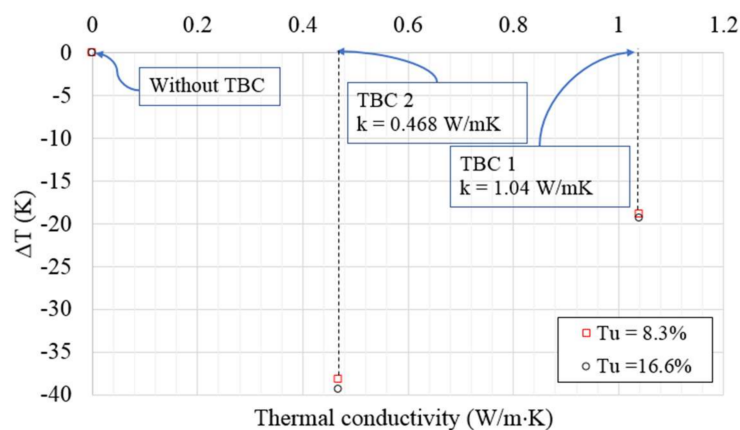

Figure 17. Reductions of average vane temperature at *Tu* = 8.3% and 16.6%.

6. Conclusions

The numerical investigation of cooling performances of a non-film-cooled turbine vane coated with a thermal barrier coating are conducted at the different *Tu*s of *Tu* = 8.3% and 16.6% using 3D CHT analysis. Through the analysis and discussion of the overall effectiveness, TBC effectiveness, heat transfer coefficient, and comparison between the vane internal temperature and average vane temperature obtained by two different TBCs, the interesting findings can be concluded as follows:

(1) At midspan, for both *Tu*s, TBC is effective in protecting the metal surface, but TBC does not play a major role near the TE. The contours indicate that at each *Tu*, the inclusion of TBC leads to the quantitative increment of overall cooling effectiveness of about 16–20%, but about 8% at the TE.

(2) At midspan, when *Tu* increases, the reduction of the metal surface temperature at midspan increases in the LE and its neighborhoods on the SS, as well as the region from the LE to the front of the TE on the PS, but hardly changes in the other regions. Also, the effective contours show that TBC alleviates the reduction of the overall effectiveness of the vane.

(3) When the level of *Tu* rises, the presence of TBC slightly dampens the heat transfer coefficient in general, and causes the lower augmentation of the heat transfer coefficient in the LE and its neighborhoods on the SS, as well as the region from the LE to the front of the TE on the PS.

(4) The use of two different TBCs indicates that the vane with the lower thermal conductivity provides the lower internal and average temperatures, but its role reduces more significantly in the TE.

(5) For both TBCs, the difference of the average temperature of the vane changes insignificantly as *Tu* increases.

Nomenclatures

c_f	specific heat capacity of mainstream and coolant (J/kg·K)
c_m	specific heat capacity of metal (J/kg·K)
c_{TBC}	specific heat capacity of TBC (J/kg·K)
h	heat transfer coefficient without TBC, between metal surface and mainstream (W/m^2·K)
h_{ref}	reference heat transfer coefficient (1135 W/m^2·K)
h_{TBC}	heat transfer coefficient with TBC, between TBC surface and mainstream (W/m^2·K)
k_f	thermal conductivity of mainstream and coolant (W/m·K)
k_m	thermal conductivity of metal (W/m·K)
k_{TBC}	thermal conductivity of TBC (W/m·K)
P	pressure (Pa)
P_{ref}	reference pressure (321.7 kPa)
$P_{s,out}$	static pressure at mainstream outlet (192.5 kPa)
$P_{t,in}$	mainstream total pressure (321.7 kPa)
q_{flux}	heat flux at the interface of solid–fluid domains (W/m^2)
R	metal temperature reduction (%)
T	metal surface temperature without TBC (K)
T_c	inlet temperature at each coolant passage (K)
T_{ref}	reference temperature (783 K)
$T_{t,in}$	mainstream total temperature (783 K)
T_{TBC}	metal surface temperature with TBC (K)
T_w	local wall temperature (K)
T_∞	inlet temperature of mainstream (K)
T'	TBC surface temperature (K)
Tu	turbulence intensity (%)
Greek symbols	
ρ_f	density of mainstream and coolant (kg/m^3)
ρ_m	density of metal (kg/m^3)
ρ_{TBC}	density of TBC (kg/m^3)
ν_f	viscosity of mainstream and coolant (kg/m·s)
φ	overall cooling effectiveness without TBC
φ_{TBC}	overall cooling effectiveness with TBC
τ	thermal barrier coating effectiveness

References

1. Meier, S.M.; Gupta, D.K. The evolution of thermal barrier coatings in gas turbine engine applications. *J. Eng. Gas Turbines Power* **1994**, *116*, 250–257. [CrossRef]
2. Maikell, J.; Bogard, D.; Piggush, J.; Kohli, A. Experimental simulation of a film cooled turbine blade leading edge including thermal barrier coating effects. *J. Turbomach.* **2010**, *133*, 011014. [CrossRef]
3. Boyle, R.J. Effects of thermal barrier coating on approaches to turbine blade cooling. In Proceedings of the ASME Turbo Expo 2006, Barcelona, Spain, 8–11 May 2006.
4. Boyle, R.J.; Senyitko, R.G. Effects of Surface Roughness on Turbine Vane Heat Transfer. In Proceedings of the ASME Turbo Expo 2005: Power for Land, Sea, and Air, Reno, NV, USA, 6–9 June 2005.

5.　Mangani, L.; Cerutti, M.; Maritano, M.; Spel, M. Conjugate heat transfer analysis of NASA C3X film cooled vane with an object-oriented CFD code. In Proceedings of the ASME Turbo Expo 2010, Glasgow, UK, 14–18 June 2010.

6.　Bianchini, C.; Facchini, B.; Mangani, L.; Maritano, M. Generic grid interface development and application to conjugate heat transfer analysis. In Proceedings of the Open Source CFD International Conference, Berlin, Germany, 4–5 December 2008.

7.　Facchini, B.; Bianchini, C.; Mangani, L. Conjugate heat transfer analysis of an internally cooled turbine blade with an object oriented CFD code. In Proceedings of the Eighth European Conference on Turbomachinery, Graz, Austria, 23–27 March 2009.

8.　Wang, Z.F.; Yan, P.G.; Huang, H.Y.; Han, W.J. Conjugate heat transfer analysis of a high pressure air-cooled gas turbine vane. In Proceedings of the ASME Turbo Expo 2010, Glasgow, UK, 14–18 June 2010.

9.　Zhang, H.J.; Zou, Z.P.; Li, Y.; Ye, J.; Song, S.H. Conjugate heat transfer investigations of turbine vane based on transition models. *Chin. J. Aeronaut.* **2013**, *26*, 890–897. [CrossRef]

10.　Na, S.; Williams, B.; Dennis, R.A.; Bryden, K.M.; Shih, T.I.-P. Internal and film cooling of a flat plate with conjugate heat transfer. In Proceedings of the ASME Turbo Expo 2007, Montreal, QC, Canada, 14–17 May 2007.

11.　Bohn, D.E.; Becker, V.J. A conjugate 3-D flow and heat transfer analysis of a thermal barrier cooled turbine guide vane. In Proceedings of the ASME the International Gas Turbine & Aeroengine Congress & Exhibition, Stockholm, Sweden, 2–5 June 1998. ASME paper 98-GT-89.

12.　Hylton, L.D.; Mihelc, M.S.; Turner, E.R.; Nealy, D.A.; York, R.E. *Analytical and Experimental Evaluation of the Heat Transfer Distribution over the Surface of Turbine Vanes*; Paper Report No. CR-168015; NASA: Washington, DC, USA, 1983.

13.　Baldwin, B.S.; Lomax, H. Thin layer approximation and algebraic model for separated turbulent flows. In Proceedings of the 16th aerospace sciences meeting, Huntsville, AL, USA, 16–18 January 1978.

14.　Bohn, D.E.; Tümmers, C. Numerical 3-D conjugate flow and heat transfer investigation of a transonic convection-cooled thermal barrier coated turbine guide vane with reduced cooling fluid mass flow. In Proceedings of the ASME Turbo Expo 2003, Atlanta, GA, USA, 16–19 June 2003.

15.　Alizadeh, M.; Izadi, A.; Fathi, A. Sensitivity analysis on turbine blade temperature distribution using conjugate heat transfer simulation. *J. Turbomach.* **2014**, *136*, 011001. [CrossRef]

16.　Yongbin, J.; Chao, M.; Bing, G.; Shusheng, Z. Conjugate heat transfer investigation on the cooling performance of air cooled turbine blade with thermal barrier coating. *J. Therm. Sci.* **2016**, *25*, 325–335.

17.　Rossette, A.H.; Mazur, Z.; Demeulenaere, A.; Hernández, J.R.L. The effect of start-up cycle in ceramic coating used as thermal barrier for a gas turbine bucket. *Appl. Therm. Eng.* **2009**, *29*, 3056–3065. [CrossRef]

18.　Spalart, P.R.; Allmaras, S.R. A one-equation turbulence model for aerodynamic flows. In Proceedings of the 30th Aerospace Sciences Meeting & Exhibit, Reno, NV, USA, 6–9 January 1992.

19.　Mayhew, J.E.; Baughn, J.W.; Byerley, A.R. The effect of freestream turbulence on film cooling adiabatic effectiveness. *Int. J. Heat Fluid Flow* **2003**, *24*, 669–679. [CrossRef]

20.　Ou, S.; Han, J.C. Influence of mainstream turbulence on leading edge film cooling heat transfer through two rows of inclined film slots. *J. Turbomach.* **1991**, *114*, 724–733. [CrossRef]

21.　Ekkad, S.V.; Du, H.; Han, J.C. Local heat transfer coefficient and film effectiveness distributions on a cylindrical leading edge model using a transient liquid crystal image method. *J. Flow Visualization Image Process.* **1996**, *3*, 129–140. [CrossRef]

22.　Ames, F.E. *Experimental Study of Vane Heat Transfer and Aerodynamics at Elevated Levels of Turbulence*; Report No. CR-4633; NASA: Washington, DC, USA, 1994.

23.　Ames, F.E. *Experimental Study of Vane Heat Transfer and Film Cooling at Elevated Levels of Turbulence*; Report No. CR-198525; NASA: Washington, DC, USA, 1996.

24.　Thole, K.A.; Radomsky, R.W.; Kang, M.B.; Kohli, A. Elevated freestream turbulence effects on heat transfer for a gas turbine vane. *Int. J. Heat Fluid Flow* **2002**, *23*, 137–147. [CrossRef]

25.　Repko, T.W.; Nix, A.C.; Heidmann, J.D. A parametric numerical study of the effects of freestream turbulence intensity and length scale on anti-vortex film cooling design at high blowing ratio. In Proceedings of the ASME Heat Transfer Summer Conference 2013, Minneapolis, MN, USA, 14–19 July 2013.

26.　Dyson, T.E.; Bogard, D.G.; Bradshaw, S.D. A CFD evaluation of multiple RANS turbulence models for prediction of boundary layer flows on a turbine vane. In Proceedings of the ASME Turbo Expo 2013, San Antonio, TX, USA, 3–7 June 2013.

27.　Foroutan, H.; Yavuzkurt, S. A model for simulation of turbulent flow with high free stream turbulence implemented in OpenFOAM®. *J. Turbomach.* **2013**, *135*, 031022. [CrossRef]

28.　Morata, E.C.; Gourdain, N.; Duchaine, F.; Gicquel, L.Y.M. Effects of free-stream turbulence on high pressure turbine blade heat transfer predicted by structured and unstructured LES. *Int. J. Heat Mass Transf.* **2012**, *55*, 5754–5768. [CrossRef]

29.　Davidson, F.T.; Dees, J.E.; Bogard, D.G. An experimental study of thermal barrier coatings and film cooling on an internally cooled simulated turbine vane. In Proceedings of the ASME Turbo Expo 2011, Vancouver, BC, Canada, 6–10 June 2011.

30.　Prapamonthon, P.; Xu, H.Z.; Ke, Z.Q.; Yang, W.S.; Wang, J.H. Thermal barrier coating and turbulence intensity effects on leading edge cooling using conjugate heat transfer analysis. *Trans Can. Soc. Mech. Eng.* **2017**, *41*, 249–263.

31.　Prapamonthon, P.; Xu, H.Z.; Yang, W.S.; Wang, J.H. Numerical study of the effects of thermal barrier coating and turbulence intensity on cooling performances of a nozzle guide vane. *Energies* **2017**, *10*, 362. [CrossRef]

32.　Halila, E.E.; Lenahan, D.T.; Thomas, T.T. *High Pressure Turbine Test Hardware Detailed Design Report*; Report CR-167955; NASA Lewis Research Center: Cleveland, OH, USA, 1982.

33.　Wang, X.Y.; Guo, S.N.; Zhao, L.L.; Zhu, Y.P.; Ai, L. A novel thermal barrier coating for high-temperature applications. *Ceram. Int.* **2016**, *42*, 2648–2653. [CrossRef]

34.　Wang, X.Y.; Zhua, Y.P.; Dua, L.Z.; Zhang, W.G. The study on porosity and thermophysical properties of nanostructured La2Zr2O7 coatings. *Appl. Surf. Sci.* **2011**, *257*, 8945–8949. [CrossRef]

35.　Feuerstein, A.; Knapp, J.; Taylor, T.; Ashary, A.; Bolcavage, A.; Hitchman, N. Technical and economical aspects of current thermal barrier coating systems for gas turbine engines by thermal spray and EBPVD: A Review. *J. Therm. Spray Technol.* **2008**, *17*, 199–213. [CrossRef]